

## Supporting Information

### Solid-State Cation Exchange Reaction to Form Multiple Metal Oxide Heterostructure Nanowires

Y. Hsuan Chen<sup>a†</sup>, Chun-Wei Huang<sup>a†</sup>, Ping-Hung Yeh<sup>b</sup>, Jui-Yuan Chen<sup>a</sup>, Tin-Yi Lin<sup>a</sup>,  
Chia-Fu Chang<sup>a</sup> and Wen-Wei Wu<sup>a†</sup>

<sup>a</sup>Department of Materials Science and Engineering, National Chiao Tung University,  
Hsinchu 300, Taiwan

<sup>b</sup>Department of Physics, Tam Kang University, New Taipei 251, Taiwan

\*corresponding author: [wwwu@mail.nctu.edu.tw](mailto:wwwu@mail.nctu.edu.tw)

<sup>†</sup>Y. H. Chen and C. W. Huang contributed equally to this work

#### List of Contents.

Table S1 | The table of plane distance comparison of Al<sub>2</sub>O<sub>3</sub> and ZnO

Table S2 | Structural comparison between  $\kappa$ -Al<sub>2</sub>O<sub>3</sub> and  $\alpha$ -Al<sub>2</sub>O<sub>3</sub>

Figure S1 | The illustration for procedure of TEM sample and photo-sensing device.

Figure S2 | A plot of average crystal radial diameter by ZnO NW diameter.

Figure S3 | The Al<sub>2</sub>O<sub>3</sub> and ZnO lattice interface

Figure S4 | Distortions of the Al<sub>2</sub>O<sub>3</sub> lattice

Figure S5 | A TEM image of Al<sub>2</sub>O<sub>3</sub> and adjacent dark-color regions

Figure S6 | Plot of length of reaction Al<sub>2</sub>O<sub>3</sub> as a function of time.

Figure S7 | HRTEM and HAADF STEM defect images

Figure S8 | The responsivity for heterostructure ZnO/Al<sub>2</sub>O<sub>3</sub> and ZnO

Table S1. Plane distance comparison of critical planes of  $\kappa$ -Al<sub>2</sub>O<sub>3</sub> and ZnO.

	$\kappa$ -Al <sub>2</sub> O <sub>3</sub>		ZnO	
d-space	200	03-1	0001	1-100
reference (nm)	0.242	0.265	0.520	0.280
present work (nm)	0.257	0.269	0.521	0.276

Table S2. Structural comparison between  $\kappa$ -Al<sub>2</sub>O<sub>3</sub> and  $\alpha$ -Al<sub>2</sub>O<sub>3</sub>

		$\kappa$ -Al <sub>2</sub> O <sub>3</sub>	$\alpha$ -Al <sub>2</sub> O <sub>3</sub>
structure		Orthorhombic	Rhombohedral
Cell Parameter	a	4.843 Å	4.764 Å
	b	8.330 Å	4.764 Å
	c	8.954 Å	13.009 Å
Static Dielectric Constant		10.99 <sup>[1]</sup>	9.72 <sup>[1]</sup>
thermal conductivity With(fraction porosity 0.3 $\mu$ m)		0.1(W.cm <sup>-1</sup> K-1) <sup>[2]</sup>	0.075(W.cm <sup>-1</sup> K-1) <sup>[2]</sup>

The ZnO NWs were grown on Si wafer through vapor-liquid-solid mechanism; we cut the wafer into pieces, then soaked one of it into ethanol, and vibrating it to let the NWs detached from the substrate by sonication. The ethanol with ZnO NWs, was dropped onto the TEM observation samples. In order to make sure the right amount of NWS on the membrane (too much, the NWs tend to overlap or entangle; too little, no enough observed sample), we tried to cut Si substrate into similar size, and control the amount of ethanol; to make the liquid look a little turbid and appear slightly blue. Finally, we checked there's proper amount of NWs on the membrane through OM.

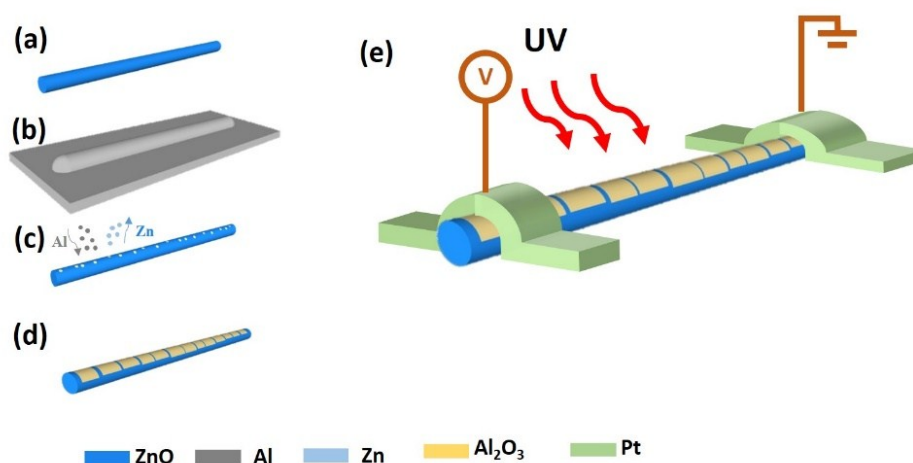


**Figure S1.** A schematic of the device fabrication process.

In this experiment, the maximum cation reaction radius of the  $\text{Al}_2\text{O}_3$  at different diameters template zinc oxide not more than 50 nm, even the film thickness of the Al metal at the same thickness. Figure S2 (a) shows the average crystals radial diameter about 40 nm with 110 nm thickness of Zn template.

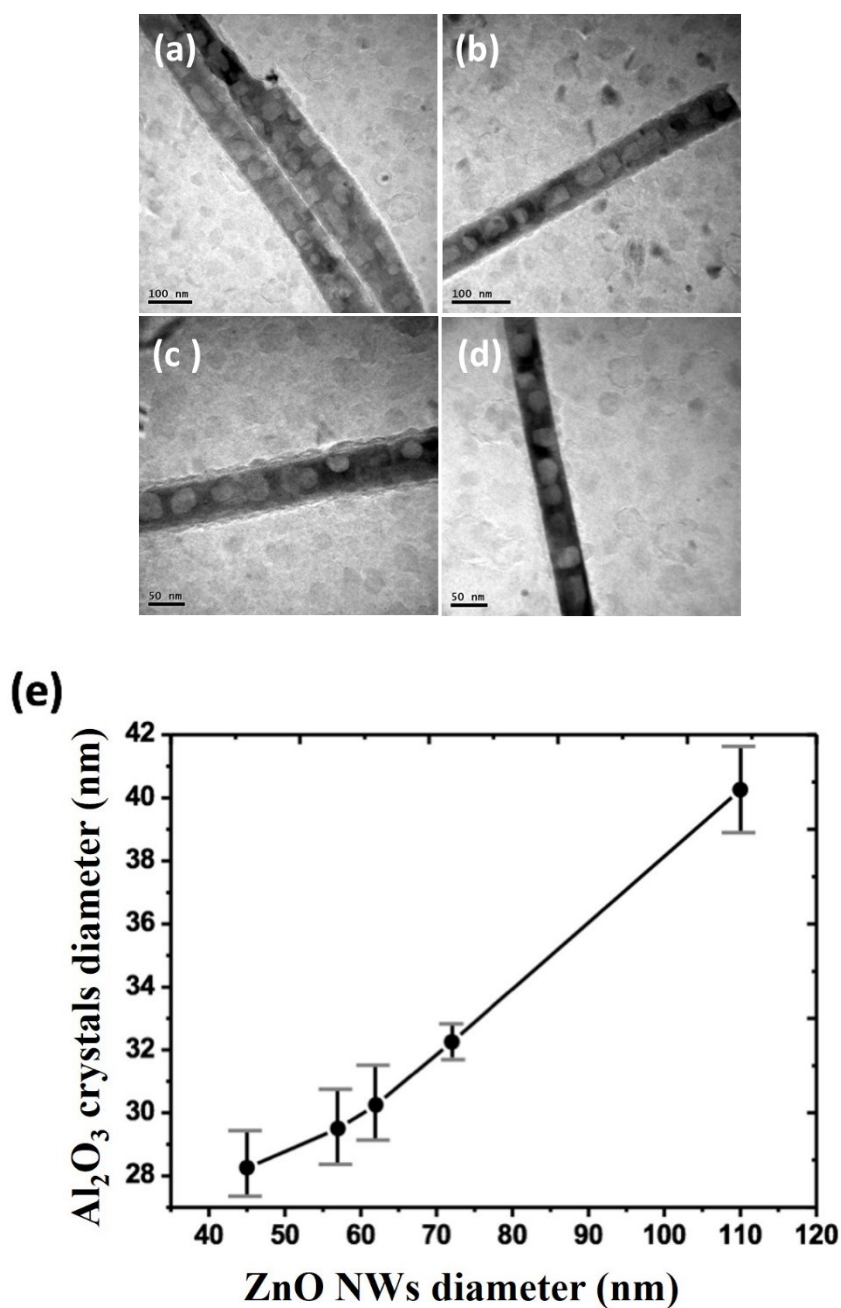


**Figure S2.** (a-d) Other ZnO/ $\text{Al}_2\text{O}_3$  multiple heterostructure nanowires (NWs). (e) Plot of average  $\text{Al}_2\text{O}_3$  crystals diameter as a function of ZnO NW diameter.

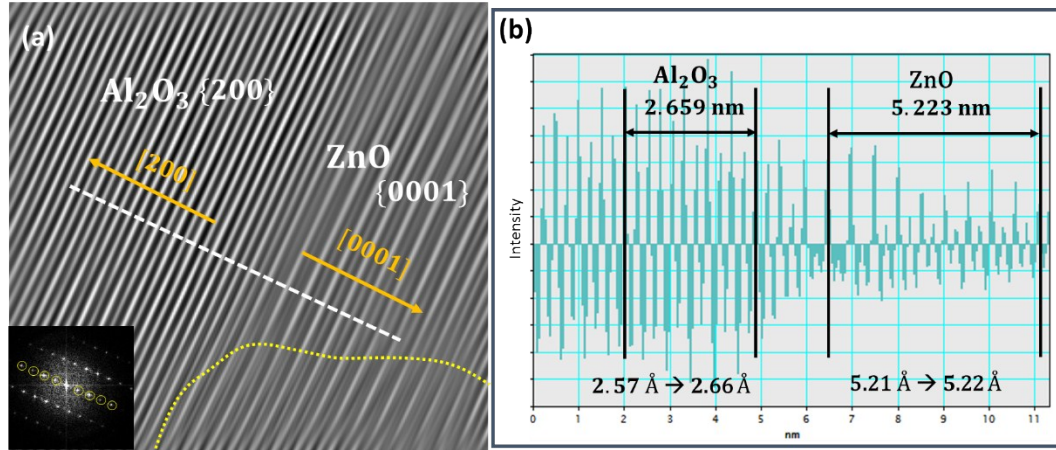


**Figure S3.** (a) To observe heterostructure epitaxy clearly, we selected specific electron diffraction points, as indicated in the inset, and used reverse FFT to obtain the filter FFT image, which revealed only  $\text{Al}_2\text{O}_3$  {200} and  $\text{ZnO}$  {0001}. The dotted line indicates the position of the plane-distance measurement shown in (b). (b) The plane distance of  $\text{Al}_2\text{O}_3$  {200} and  $\text{ZnO}$  {0001} near the interface. The average plane distance of  $\text{Al}_2\text{O}_3$  {200} is 2.66 Å. Compared with lattice relatively far from the interface shown in Figure 2c, lattice near the interface is 3.5% larger. This result illustrates that the  $\text{Al}_2\text{O}_3$  lattice tended to match up with the  $\text{ZnO}$  lattice, whereas the  $\text{ZnO}$  lattice essentially remained the same.

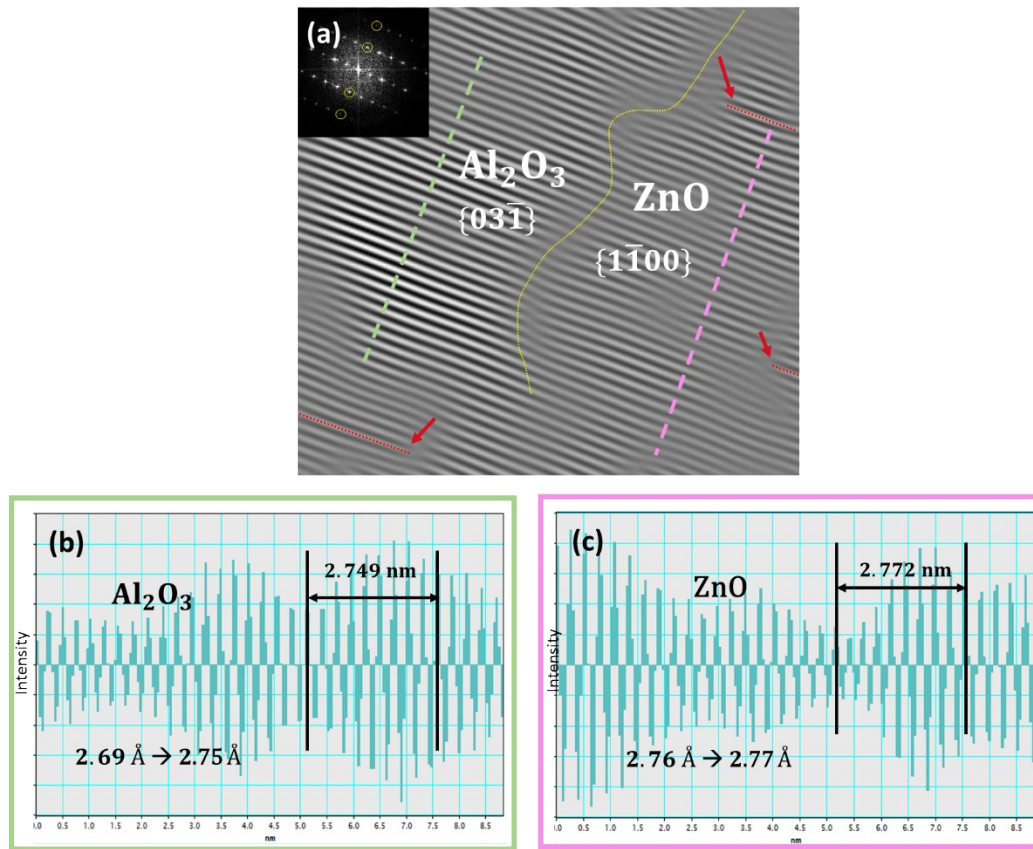


**Figure S4.** (a) We selected specific electron diffraction points, as indicated in the inset, and used reverse FFT to obtain the filter FFT image, which revealed only  $\text{Al}_2\text{O}_3$  {031} and  $\text{ZnO}$  {1100}. The yellow dotted line indicates the position of the interface, which shows slight lattice distortion. The red arrows indicate the misidentified dislocations, which were generated to release the strain of lattice mismatch. The dotted lines indicate the position of the plane-distance measurements shown in (b, c), and correspond by color. (b) The plane-distance measurement of  $\text{Al}_2\text{O}_3$  {031} near the interface. The average plane-distance of  $\text{Al}_2\text{O}_3$  {031} is 2.75 Å. We discovered results similar to those shown in Figure S3;  $\text{Al}_2\text{O}_3$  lattice near the interface is 2.2% larger than lattice far from the interface. (c) The plane-distance measurement of  $\text{ZnO}$  {1100} near the interface. The average plane-distance is 2.77 Å, and no obvious lattice differences were observed with respect to distance from the interface.

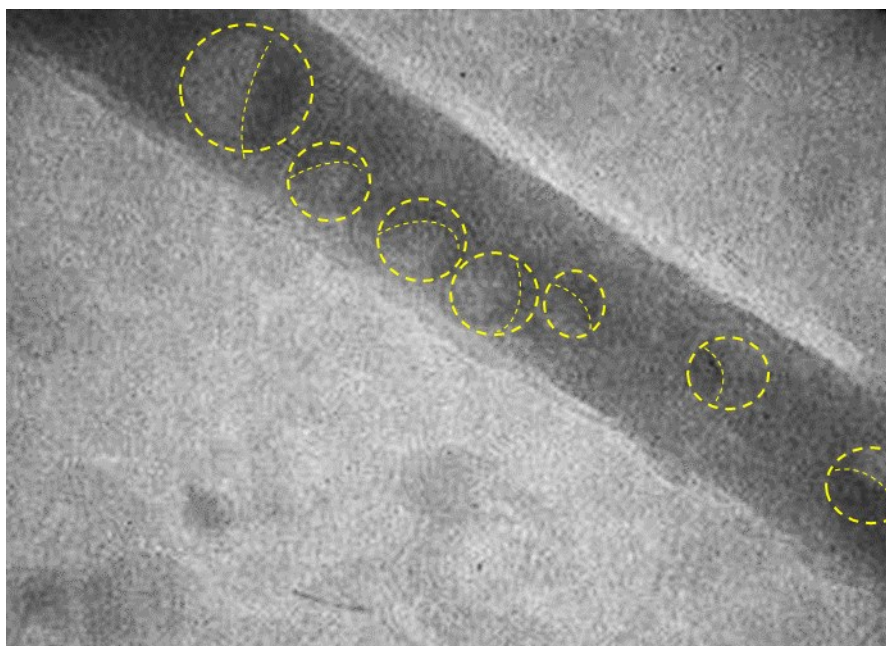


**Figure S5.** An in situ TEM image taken from a video with higher magnification at reaction time 03:30. The dotted lines indicate the formation of  $\text{Al}_2\text{O}_3$  and the adjacent dark-color regions.

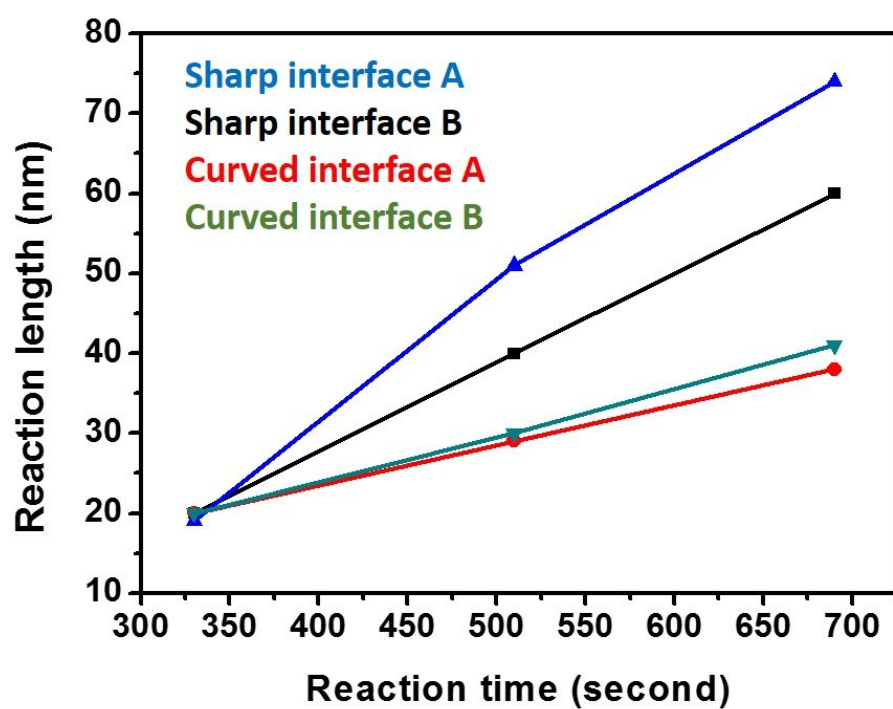


**Figure S6.** Plot of length of reaction  $\text{Al}_2\text{O}_3$  as a function of time. The sharp interfaces grow more rapidly than curved interfaces.



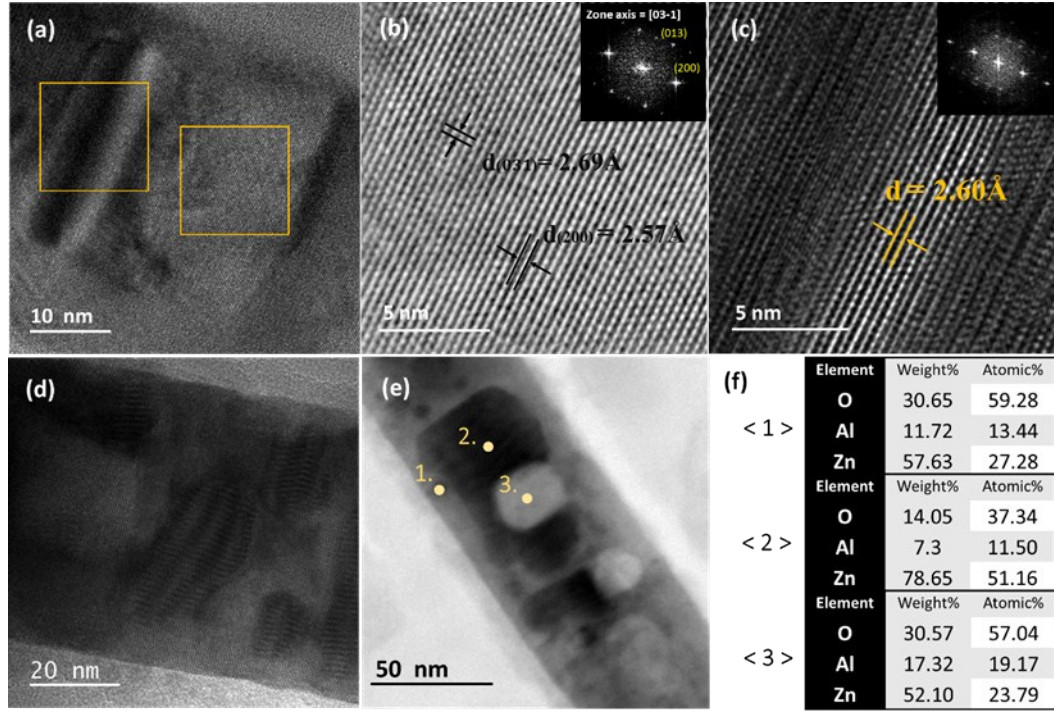
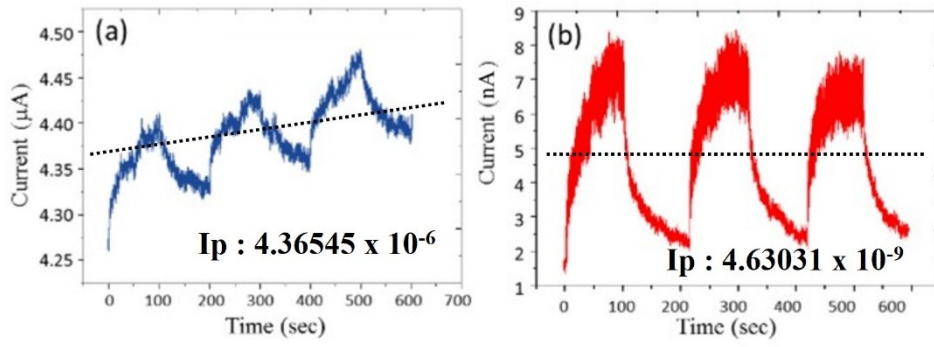


**Figure S7.** HRTEM and HAADF STEM images of defects appearing during the formation of a ZnO/Al<sub>2</sub>O<sub>3</sub> multiple heterostructure NW. (a) Low-magnification HRTEM image of a heterostructure NW. The light-color crystal (the right square) was enlarged in (b) and was identified as  $\kappa$ -Al<sub>2</sub>O<sub>3</sub> with zone axis [031]. The dark stripe beside the Al<sub>2</sub>O<sub>3</sub> crystal (the left square) is shown enlarged in (c). (b) The enlarged HRTEM image of the right square in (a) was identified as Al<sub>2</sub>O<sub>3</sub> with zone axis [031]. (c) The enlarged HRTEM image of the left square in (a). The plane distance of the light-color stripe is 2.6 Å, which suggests  $\kappa$ -Al<sub>2</sub>O<sub>3</sub>. In the dark stripe region, some additional planes were being inserted into the main lattice. According to the information above and the dynamic dark stripes observed from in situ video, we suggest that the excess zinc ions induced the mixed Al<sub>2</sub>O<sub>3</sub> lattice that showed dark TEM imaging contrast. (d) The TEM image of the heterostructure NW with Moiré fringes. (e, f) The HAADF image of the heterostructure NW with Moiré fringes and corresponding point analysis. According to the point analysis, point 3 is likely a small crystalline Al<sub>2</sub>O<sub>3</sub> region, and it illustrates that the reaction was stopped in its early stage due to nonuniform TEM sample heating. The Moiré fringe regions show significant high percentages of zinc and lower oxygen percentages than the other regions; therefore, we suggest that high concentration of zinc ions crystallized into Zn crystals after cooling, and then induce the Moiré fringes in TEM imaging.



$$R = \frac{I_p}{P_{output}} (\mu A/w)$$

**Figure S8** The responsivity for heterostructure ZnO/Al<sub>2</sub>O<sub>3</sub> and ZnO was  $R_{Heter} : 1.475 \mu A/w$  and  $R_{ZnO} : 1390 \mu A/w$ , respectively. The heterostructure had good sensitivity but normal responsivity due to its structure with lower current value.

#### Reference

1. C. K. Lee, E. Cho, H. S. Lee, K. S. Seol, and S. Han, Physical Review B, 2007, **76**, 245110.
2. E. J. Gonzaleza, G. Whitea and L. Weia, Journal of Materials Research, 2000, **15**, 744-750.